Signal Design and Processing Techniques for WSR-88D Ambiguity Resolution

Staggered PRT Technique

National Severe Storms Laboratory Report

prepared by: M. Sachidananda
with contributions by: D. S. Zrnic´ and R. J. Doviak

Part 4
October 2000

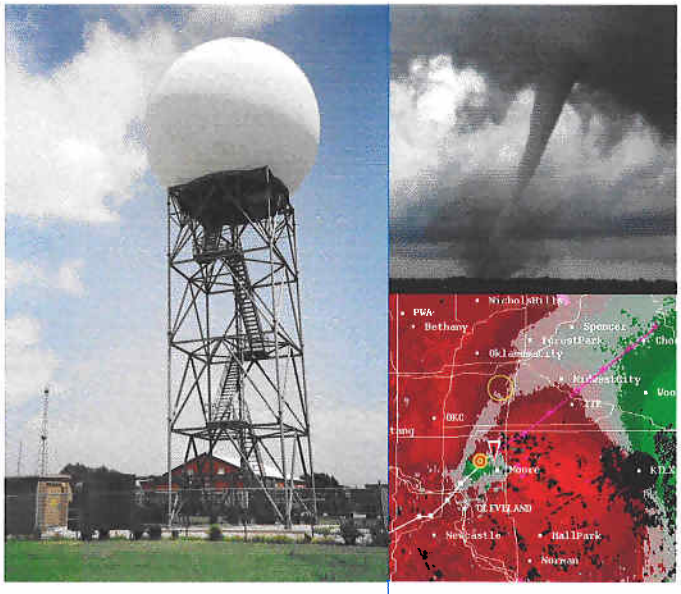

National Oceanic and Atmospheric Administration
National Severe Storms Laboratory
Norman, Oklahoma 73069

SIGNAL DESIGN AND PROCESSING TECHNIQUES FOR WSR-88D AMBIGUITY RESOLUTION

PART - 4: Staggered PRT Technique

National Severe Storms Laboratory Report

prepared by: M. Sachidananda,
with contributions by: D.S. Zrnic and R.J. Doviak

October 2000

NOAA, National Severe Storms Laboratory
1313 Halley Circle, Norman, Oklahoma 73069

SIGNAL DESIGN AND PROCESSING TECHNIQUES FOR WSR-88D AMBIGUITY RESOLUTION
Part-4: staggered PRT

Contents

ooo000ooo

SIGNAL DESIGN AND PROCESSING TECHNIQUES FOR WSR-88D AMBIGUITY RESOLUTION

Part - 4: the staggered PRT technique

1. Introduction

The Operational Support Facility (OSF) of the National Weather Service (NWS) has funded the National Severe Storms Laboratory (NSSL) to address the mitigation of range and velocity ambiguities in the WSR-88D. This is the fourth report in the series that deals with velocity and range ambiguity resolution in the WSR-88D. The first two reports mainly dealt with uniform PRT transmission and phase coding techniques to resolve the range ambiguity. Although the phase coding techniques do not directly address the velocity ambiguity problem, their capability to separate overlaid echoes allows the use of shorter PRTs which, in turn, diminishes the occurrence of ambiguous velocities. In the third part, we considered the staggered PRT technique and its variants. The significant results in the Report 3 are a new staggered PRT sequence processing scheme in the spectral domain which significantly improves spectral moment estimates, and a clutter filtering method that recovers velocity information over the entire extended unambiguous velocity interval without any drop-out regions. The only assumption made in the algorithm is that there is no overlaid signal. This necessarily restricts the selection of the PRT T_1 to be sufficiently large for a given elevation so that the probability of overlay is small.

After the third report was submitted in July 1999, some more ideas were explored in an effort to further improve the staggered PRT scheme. Specifically, we tried to further improve the velocity estimate errors by optimizing the window weights. We also examined the possibility of increasing the unambiguous range to r_{a2}, by resolving the overlaid signal from corresponding to the shorter range r_{a1}. Exhaustive simulations were carried out to evaluate the performance of the staggered PRT decoding scheme and determine the limits of

spectral moment recovery within acceptable bonds under various conditions. This information is very useful in developing a data censoring strategy to discard or flag the bad data. The results from all these studies has been reported in this Part-4 of the report. In the light of these new results and an enhanced capability of the staggered PRT algorithm, we have revised the proposed WSR-88D scan strategy given in Table.5.3 of Report 3. The notations used in this report are the same as in Report 3. This study is essentially a continuation of the staggered PRT work. A brief introduction to the staggered PRT technique was given in Report 3, and a part of it is repeated here for the convenience of readers and to recall the symbols and notations used in the context of the staggered PRT processing.

2. The staggered PRT technique

Here, we describe the staggered PRT scheme briefly before we embark on a discussion of the new method of processing. In the staggered PRT technique (Zrnic and Mahapatra, 1985), two different pulse spacings, T_1 and T_2; ($T_2>T_1$), are used alternately (Report 3, Fig. 2.1a). Then, alternate pairs of return samples are used to compute autocorrelation estimates, R_1 at lag T_1 and R_2 at lag T_2. The velocity is estimated from the phase difference between the two using the formula,

$$\hat{v} = \lambda \, arg(R_1 R_2^*) \, / \, [4\pi(T_2-T_1)] \, . \qquad (2.1)$$

Thus, the difference in PRT, (T_2-T_1), determines the unambiguous velocity, v_a, for the staggered PRT technique and is given by

$$v_a = \pm \lambda \, / \, [4(T_2-T_1)] \; ; \;\; T_1 < T_2 \, . \qquad (2.2)$$

Zrnic and Mahapatra (1985) suggest a procedure to estimate mean velocity and signal power for echoes received within the time delay (T_1+T_2). In theory, this seems to be possible because the overlaid signals in any two consecutive samples are from two different

ranges and, therefore, are uncorrelated. Thus, the expected value of the overlaid signal contribution to the autocorrelation is zero, and the effective unambiguous range becomes

$$r_a = c(T_1+T_2)/2. \qquad (2.3)$$

Eq. 2.1 and 2.3 suggest that the staggered PRT is equivalent to a uniform PRT = (T_1+T_2) for the unambiguous range and a uniform PRT, $T_u = (T_2-T_1)$ for the unambiguous velocity, and each can be selected independently. However, the practical utility of this scheme is limited due to the quality of estimates. The overlaid signal increases the variance of the estimates because it acts as noise. Thus, the ratio of the overlaid signal powers is the equivalent signal-to-noise ratio (SNR), and for a reasonable accuracy of the estimates, the unwanted signal has to be at least 3 dB below the desired signal power.

Let $r_{a1} = cT_1/2$ and $r_{a2} = cT_2/2$ so that $r_a=r_{a1}+r_{a2}$, and $r_{a1} < r_{a2}$. If r_{a1} is chosen sufficiently large so that no echoes are received from ranges greater than r_{a1}, then the problem of overlaid echoes could be eliminated. If we choose PRTs such that we have no echoes from range greater than r_{a2} then for some of the range gates, the alternate samples have overlaid signal from another range gate separated by a delay time T_1, and the rest are free of overlaid signal. This situation, we call the "one-overlay" situation, is thought to be a good candidate for further extending the unambiguous range to r_{a2}, with some additional processing. This possibility has been explored in this report.

It is shown by Zrnic and Mahapatra (1985) that the standard error in the velocity estimate increases as the ratio $\kappa = T_1/T_2$ approaches unity, and a good choice is κ =2/3. Thus, the unambiguous range and unambiguous velocity are indirectly tied in practice via the estimate accuracy. However, compared to the uniform PRT, it is possible to achieve a much larger r_a and v_a because the limiting equation is $v_a\, r_{a2} = \{1/(1-\kappa)\}c\lambda/8$ for the staggered PRT scheme with one-overlay resolution. Report 3 indicates that κ =2/3 is optimum irrespective of the decoding algorithm, hence in this study we examine the κ =2/3 case only. Some discussion on other values of κ is available in Report 3.

3. Review of the staggered PRT sequence processing

The estimation of the spectral moments of the weather echo from the staggered PRT sequence is based on a few key ideas. The first idea is to view the non-uniform sample sequence as a product of a uniform sample sequence and a binary code sequence. Thus, the spectrum of the staggered PRT sequence can be viewed as a convolution in the spectral domain. Because of the singular nature of the convolution matrix, the de-convolution cannot be carried out. However, under certain conditions of narrow weather spectra, "magnitude de-convolution" can recover the spectral magnitudes, but not the complex coefficients (Sachidananda and Zrnic 2000). The phases are not required for estimating the spectral moments. Thus, the velocity estimation is identical to that of the pulse pair processing, except that the autocorrelation is not computed using the pairs of pulses but from the power spectrum. One of the major advantages of this procedure is that the standard errors in the velocity estimates are much lower than errors in estimates obtained by the conventional pulse pair processing. This comes about because, in the pulse pair processing of staggered PRT data (Zrnic and Mahapatra 1985), autocorrelations are computed at two different lags, T_1 and T_2, and the phase difference is used for computing the velocity, whereas in the new approach the autocorrelation for lag $(T_2 - T_1)$ is directly computed. Incidentally, this is a spin-off from the approach that we adopted to filter the clutter from the staggered PRT sequence. When the staggered PRT work was undertaken a method for clutter filtering was sought, because that was one of the major hurdles which prevented implementation of the staggered PRT technique in operational radars.

The second idea, central to the filtering of the clutter from the staggered PRT sequence, is a technique to recover the spectral coefficients of the weather signal in the region where the clutter and signal are overlapping in the spectral domain. Any conventional filtering technique cannot distinguish between the signal and the clutter power in a given spectral coefficient, and filtering one would automatically eliminate the other too. In this new procedure, the modulation properties of the code sequence, under the narrow spectra condition, are utilized to retain some fraction of the signal power while filtering the clutter power completely. An estimate of the complex clutter spectral coefficient is first obtained by

projecting the complex spectral code vector (appropriate column vector of the convolution matrix) onto a set of spectral coefficients where clutter is expected (5 coefficients for κ=2/3), and this estimated clutter vector is subtracted from the set of coefficients. Because of the linear independence between the different spectral code vectors, not all the weather signal power is filtered, except when the weather signal velocity also is close to zero (ground clutter is always around zero Doppler), and this residual signal power (and some additional information) is used to restore the signal to its original value. This is possible, because the residual power left in the spectral coefficient after the clutter is filtered is a known fraction of the original signal power. The correction factor can be easily computed provided the location of the original signal component can be determined. This is accomplished by obtaining an approximate velocity estimate with the partial signal power. The procedure fails only when the clutter filter is very wide and the approximate initial velocity estimate is not within $\pm v_d/5$ of the actual value. Without this last step, which is termed the "bias removal procedure", the velocity estimate is slightly biased because of the loss of signal power from the region of the spectrum from where the clutter is filtered. This bias becomes significant for larger clutter filter widths. The upper limit for the number of coefficients from which clutter can be filtered is a little more than half the number of the total spectral coefficients, and is generally sufficient to recover velocity in the presence of clutter as large as 50dB more than the signal power. If the clutter-to-signal ratio (CSR) is lower, a narrower clutter filter would be sufficient, and for sufficiently narrow clutter filter widths (e.g., n_c<7 for a number of T_u intervals N=160, and a number of staggered samples M=64), the bias correction may not even be necessary (for CSR less than about 15 dB). A very brief account of the spectrum reconstruction and the clutter filtering procedure is given below in the next two sub-sections to provide continuity for the reader.

3.1. Reconstruction of the signal spectrum

As indicated earlier in the introduction, unless indicated otherwise the stagger ratio, κ=2/3, is assumed in all our discussions and results in this report. If T_1 and T_2 are the PRTs, we select $T_1=2T_u$, and $T_2=3T_u$. Therefore, a uniform sample sequence can be

constructed for the sampling period T_u; then the corresponding code is 10100... etc., with ones representing the samples available, and the zeros, the missing samples. If the first sample is from the T_2 pulse transmission the code would be 10010... etc. If e_i is the uniform sample sequence and c_i is the code sequence, then the available stagger PRT sample sequence, v_i, can be written as

$$v_i = c_i\, e_i \;; \qquad i=1,2,3,\ldots N\,, \tag{3.1}$$

and in the transform domain this is a convolution represented by

$$\mathrm{DFT}(\, v_i\,) = \{\, \mathrm{DFT}(\, c_i\,) \star \mathrm{DFT}(\, e_i\,)\,\} \tag{3.2}$$

where the $\star$ represents circular convolution, and the DFT( ) represents the discrete Fourier transform of the sequence in brackets. N is the number of samples after inserting zeros for the missing samples. If M is the number of staggered PRT samples, then $N=5M/2$ for $\kappa=2/3$. We use capital letters to denote the spectral coefficients, and the corresponding time domain quantities are denoted by lowercase letters. The bold face letters denote matrices. Subscript index 'i' is used for the time domain quantities, and subscript index 'k' is used for the spectral coefficients. For example, $E_k = \mathrm{DFT}(e_i)$, are the spectral coefficients, and $\mathbf{E}$ is the column matrix of coefficients E_k. Eq. (3.2) can be written in matrix form as

$$\mathbf{V} = \mathbf{C}\,\mathbf{E}. \tag{3.3}$$

$\mathbf{V}$ and $\mathbf{E}$ are (Nx1) column matrices containing the spectral coefficients, V_k and E_k, of the corresponding time sequences, v_i and e_i, and $\mathbf{C}$ is the convolution matrix (size: NxN) whose column vectors are cyclically shifted versions of C_k. Because the convolution matrix is singular, we recover the magnitude spectrum using the magnitude deconvolution defined by

$$abs\{\mathbf{E}\} = [\; abs\{\mathbf{C}\}]^{-1}\; abs\{\mathbf{V}\}, \tag{3.4}$$

where $[\ abs\{\mathbf{C}\}]^{-1}$ is the magnitude deconvolution matrix. This reconstructs the exact magnitude spectrum only under the condition of "narrow" spectra; that is, the non-zero spectral coefficients of the signal e_i are spread at most $N/5$ coefficients, or the total spread is less than $2v_a/5$ for $\kappa=2/3$ (see Report 3 or Sachidananda and Zrnic 2000).

Once the magnitude spectrum is obtained, the spectral domain equivalent of the pulse pair algorithm can be used to estimate the mean power, p, mean velocity, v, and spectrum width, w. If the ground clutter is present, the echo time series is filtered using the procedure described briefly in the next sub-section, and then the magnitude deconvolution is applied.

3.2. Ground clutter filtering

The clutter filter capitalizes on the cyclic property of the convolution matrix and the assumption that the weather signal spectra are "narrow" (as defined earlier). The code spectrum has only 5 non-zero coefficients spaced 1/5th of the total (unambiguous velocity) span, hence, only 5 spectral coefficients will be involved at a time in the convolution process. Specifically, the power in each spectral coefficient is spread over these 5 coefficients, hence the problem of clutter filtering or the spectrum reconstruction can be split into $N/5$ equations with 5 variables each, in place of one equation with N variables. For example the equation

$$\mathbf{V}_r = \mathbf{C}_r\ \mathbf{E}_r, \qquad (3.5)$$

(see Report 3, Eq 3.7 for details) consisting of the rearranged matrices is a representation of $N/5$ equations together in matrix form. To understand the clutter filtering procedure it is sufficient to consider one such equation, say the k^{th} column of the matrices $\mathbf{E}_r$ and $\mathbf{V}_r$, and form a 5x5 matrix equation.

Consider an example with parameters $\kappa=2/3$, $M=64$ for which $N=160$, and let $k=1$. The corresponding equation is

$$\begin{bmatrix} V_1 \\ V_{33} \\ V_{65} \\ V_{97} \\ V_{129} \end{bmatrix} = \begin{bmatrix} C_1 & C_{129} & C_{97} & C_{65} & C_{33} \\ C_{33} & C_1 & C_{129} & C_{97} & C_{65} \\ C_{65} & C_{33} & C_1 & C_{129} & C_{97} \\ C_{97} & C_{65} & C_{33} & C_1 & C_{129} \\ C_{129} & C_{97} & C_{65} & C_{33} & C_1 \end{bmatrix} \begin{bmatrix} E_1 \\ E_{33} \\ E_{65} \\ E_{97} \\ E_{129} \end{bmatrix}. \quad (3.6)$$

The left hand side represents the convolved spectral coefficients (available from the measurement), and the coefficients E_k are for a uniform sequence of the signal plus the clutter. Under the condition of "narrow" weather spectra, only one of its five (E_1 or E_{33} or E_{65} or E_{97} or E_{129}) coefficients is non zero; the clutter can be present in the first coefficient (or in the last coefficient for a different k), because the clutter is at zero Doppler. The amplitude and the position of the signal coefficient that we are trying to recover is not known. Then it can be shown that the column vector, **V**, on the left is E_l times the first column vector of the convolution matrix, $\mathbf{C}_r$, plus the signal spectral coefficient (whichever is non zero) multiplied by the corresponding column vector of $\mathbf{C}_r$. Therefore, if we estimate the complex amplitude of the first column vector of $\mathbf{C}_r$ present in **V** and subtract it, all the clutter is removed. However, because of the non-orthogonality of the columns of $\mathbf{C}_r$, part of the signal power is also removed (signal is completely removed when it is also in the first coefficient, or at the zero Doppler). That is, the projection of the signal vector on to the clutter vector is also removed. The remaining part of the signal has certain relationship to the original signal and hence the original signal can be recovered using the bias removal procedure (see Report 3 for details).

3.3. Studies on the effect of windows

In most of the results presented in Report 3, the von Hann window was used. It is well known that the spectral moment estimates obtained by pulse pair processing have lower standard errors without the window (i.e., uniform weights) than with the window, because of the loss of power due to the window weights. The window becomes necessary to contain the clutter signal from spreading across the spectrum, and also for the spectrum width computation after magnitude deconvolution. This is a non-linear procedure, and it is difficult to compute the effect of window on the standard error in the width estimate theoretically. In the previous study, no effort was made to optimize the performance of the algorithm with respect to the window function. Here we examine this problem in more detail using simulation results to estimate standard errors and biases in the spectral moment estimates. First we evaluate the optimum window to be used when the clutter is absent, and later we examine the case with clutter. The optimum is different for these two cases.

3.3.1. Spectral moment estimation in the absence of ground clutter

The standard errors in the spectral moment estimates depend on several factors such as the wave length, PRTs, number of samples, spectrum width, etc. It is not easy to present all the data on the variation of the *sd(v)* with respect to all these parameters, nor is it necessary. Here, we consider the values relevant to the WSR-88D. In the vcp-11 (see Table.5.1a, Report 3), the complete volume scan takes about 5 minutes to cover the 14 elevations. For each radial, the dwell time is about 51 ms for lowest two elevations, and it is about 40 ms for higher elevations. With the sample overlap scheme (see Report 2, page-71), it is possible to reduce *sd(v)* by taking about 30 per cent overlapping samples. With rectangular window, this will result in an increased azimuthal smoothing of the velocity field (and other parameters), but with the von Han window the smoothing is marginal.

The pulse pair processing gives better estimates without the window (rectangular window is inherent), but, for width estimation, the window is required to avoid biased estimates. There are different estimators available for width estimation, but the one given by equation (6.27) of Doviak and Zrnic (1993) has the lowest standard error, and this estimator

produces a bias for low spectrum widths. This can be removed if window weighting is used. Of course, we have the option of using the window only for width estimation at the expense of more computation. The increase in the *sd(v)* appears to be related to the power loss due to the window. Hence, we examined different weighting functions, specifically the (von Hann)^p weights, and evaluated the performance of the algorithm. The exponents used are p=0, 0.25, 0.5, 1, and 2 (p=0 corresponds to no window or the rectangular window). A large number of simulations were carried out to obtain the standard error and the bias error in the mean power, the mean velocity and spectrum width estimates. These are in Figs. 3.1 to 3.3 for the three parameters; the mean of the simulation data is smoothed (curve fitted) for clarity. The simulation parameters are indicated in the figures. It can be seen that the spectrum width has a significant bias without the window (Fig. 3.1), but for all other windows, the bias is almost zero. We have examined exponents less than 0.25, but the bias could not be removed fully. The lowest exponent that works well is 0.25, which has a power loss factor of 1.93 dB. Power losses inherent to the von Hann window with the exponents, p = 0, 0.25, 0.5, 1, and 2, are 0, 1.93, 2.98, 4.23, and 5.6 dB, respectively. The *sd(v)* plot (Fig.3.2) indicates that the *sd(v)* for the first two cases is almost the same, and in fact, the second curve for exponent 0.25 is better in terms of the bias error for large spectrum widths. The mean power estimate (Fig.3.3) is best without the window (i.e., with rectangular window). Therefore, we conclude that the best method to adopt in the staggered PRT algorithm is, the mean power estimation using the time series samples directly, no window for the velocity estimation, and for width estimation (von Hann)$^{0.25}$ weighted time series. This, of course, increases the computation, because the FFT and magnitude deconvolution have to be carried out twice, with and without the window weights. But, because the degradation in the velocity estimate is marginal with (von Hann)$^{0.25}$ window, we can use it for both velocity and width estimation, thus, avoid one extra FFT and deconvolution operation.

The choice of PRTs determines the unambiguous range r_{al} as well as the number of samples available in a given dwell time. As mentioned earlier, the vcp-11 uses two dwell times, these are approximately 40 ms and 50 ms. Therefore, the performance of the

algorithm is evaluated for these two dwell times, and is presented in the form of contour plots in Figs. 3.4a and 3.5a. (The values are listed in tables 3.1 and 3.2.) The area left of the contour is the region of lower *sd(v)*, and for a given *sd(v)*, the contour can be approximated with a straight line. From these results an empirical relation can be derived which defines the region of velocity recovery within a specified standard error for any selection of PRTs. In fact, if we plot the *sd(v)* as a function of normalized width (normalized with respect to the unambiguous velocity), we find that the curves for different v_a are nearly the same for a given dwell time, as shown in Figs. 3.4b, and 3.5b, for the same set of data given in the contour plots. If we set an upper limit of 1 m s^{-1} for *sd(v)*, maximum normalized spectrum widths for velocity recovery are $w/2v_a$=0.045 and 0.05, for dwell times 40 ms and 50 ms, respectively (from Figs. 3.4b and 3.5b). These four figures provide an idea of the overall performance of the staggered PRT algorithm. It is seen that there is an upper limit for the spectrum width of the signal beyond which the velocity cannot be recovered with sufficient accuracy, and this upper limit is directly proportional to the unambiguous velocity. Hence, we cannot select low unambiguous velocities to increase the unambiguous range.

3.3.2. Ground clutter filtering and the window

The ground clutter is generally a concern at lower elevation scans. At elevations higher than about 5° the ground clutter is not a serious problem. The WSR-88D specifies 50 dB rejection for the ground clutter with a spectrum width of 0.28 m s^{-1} centered on zero Doppler. We use a Gaussian shaped spectrum with this width for the ground clutter in our simulation study, and specify clutter-to-signal ratio (CSR) as a parameter rather than the clutter rejection. We adopt this notation because our ultimate aim is to recover the spectral moments of the weather echo, and to achieve this, it is sufficient to filter enough clutter power to get a decent SNR (i.e., signal to residual clutter) so that the spectral moment estimates are accurate. The amount of filtering required depends on the CSR. Further, the clutter suppression ratio, α, defined as the ratio of the total clutter power to the residual clutter power after filtering, expressed in dB units, is a function of the filter width, hence,

any suppression can be obtained by suitably choosing the filter width. But this does not guarantee recovery of spectral moments of the weather signal, because there is an upper limit for the filter width beyond which the velocity cannot be recovered irrespective of the CSR. There is always an optimum clutter filter width for a given CSR and a clutter spectrum width. If the clutter filter width is allowed to be adjusted in the staggered PRT decoding algorithm based on an a-priori knowledge of the CSR, the performance of the algorithm can be optimized. It is obvious that the residual clutter power is spread throughout the spectrum, hence, can be treated as an effective noise. Thus, the effective SNR_e after filtering the ground clutter is equal to (α - CSR) dB (this assumes that other noise power is very small compared to the residual clutter power). The SNR_e has to be better than 10 dB to recover velocity of the weather echo with a good accuracy.

Other parameters that play important roles in the clutter filtering are the window function and the number of available staggered PRT samples, M, because, the suppression ratio is a strong function of these two parameters. This is illustrated in Figs. 3.6 to 3.8, where the clutter suppression ratio versus the normalized clutter filter width, $\zeta=w_f/w_c$, is shown for three different sample sequence lengths. The data is obtained from a large number of simulations, and their mean values are plotted. The filter widths used are discrete (indicated by the symbols: rectangle, triangle and circles) because the filter is implemented in the spectral domain where only discrete number of coefficients can be deleted (only odd numbers are used for n_c, the filter width in terms of the number of coefficients). With the inherent rectangular window, the clutter echo spreads much more across the extended spectrum, and α has an upper limit of 20 dB even with very large filter width. Therefore, it becomes necessary to apply some window to contain the spread of the clutter power. Instead of trying different window functions available, we chose to try the von Hann window weights raised to some power. As the exponent is increased the main lobe of the spectrum of the window function widens but the side lobe level decreases. Simulations with different exponents for the von Hann weights show that the best performance is for exponents near 1 and 2, hence α for only for these two exponents is plotted in Figs. 3.6 to 3.8. The curves for the ideal Gaussian spectrum and the rectangular window are also

presented for comparison. A common feature in all three figures is that, there is a cross over point between the two curves (von Hann and {von Hann}^{2}) for some filter width. For lower filter widths von Hann window gives better clutter suppression and for larger widths the {von Hann}^{2} window gives better α. Both these curves are very sensitive to the number of samples, M, as seen by comparing the three figures. By doubling M (compare M=32 and 64) α changes by about 10 dB for von Hann window (for large filter widths) and it is as much as 25 dB for the {von Hann}^{2} window. Thus, it can be concluded that for a large CSR (which requires large w_f/w_s), the{von Hann}^{2} window is better, and for a low CSR, (low filter widths) the von Hann window is preferable. The expected amount of clutter suppression in different situations can also be seen from these three figures and therefore the ability of the algorithm to recover the velocity can be inferred. There is an upper limit for the clutter filter width that can be used (for a given M); it is M/4 coefficients for large weather spectrum widths (more than about 4 m s^{-1}). The upper limit for the clutter filter width is less than M/4 coefficients for signals with narrow spectrum widths signals if the mean velocity is close to one of the values 0, $\pm 2v_a/5$, $\pm 4v_a/5$ (m s^{-1}) (for κ = 2/3) at which the clutter and signal spectra (convolved with the code spectrum) overlap. If the two spectra do not overlap, the upper limit for the clutter filter width can still be M/4 even for w < 4 m s^{-1}. Beyond this limit the bias removal part fails, because the error in the initial estimate of the velocity exceeds the maximum allowable ($v_a/5$ for κ=2/3).

For a typical WSR-88D dwell time of approximately 40 ms, the number of staggered PRT samples is about 32, if v_a is chosen to be $\pm$50 m s^{-1} (T_u = 0.5 ms). For this M it is best to use von Hann window up to ζ = 22, and achieve a clutter suppression of 40 dB, but the filter width is almost close to the maximum allowable for this ζ. However, if a 25 per cent larger number of samples can be utilized (M=40, using the sample overlap scheme, see Report 2, page 71) without slowing down the scan rate, we can achieve an additional 5 dB suppression with the von Hann window. For the lowest two elevations where the dwell time is about 51 ms, we get 51 samples per radial with 25 per cent sample overlap. It is also possible to use a larger overlap and {von Hann}^{2} window without much degradation in the estimates. The {von Hann}^{2} window has a much larger edge taper resulting in a lower

effective smearing (for the same overlap) of the estimates in azimuth (effective number of overlapped samples is much smaller because of the weights). For M=64 or more, a {von Hann}^{2} window is a better choice, as can be seen from Fig.3.8. It can also be observed from the figures that a larger number of samples allows a better suppression of the ground clutter for the same normalized clutter filter width.

Some sample velocity plots are shown in Figs.3.9 to 3.11. The estimated velocity is shown against the velocity input to the simulation program. 20 simulations are carried out at each of the velocities spanning the entire $\pm v_a$, at intervals of 1 m s^{-1}. The dots show the simulation points, and the continuous curve is the mean. The parameters used in the simulation are indicated in the figures. The first figure, Fig.3.9, is with M=32 and CSR=35 dB, which is almost the maximum limit for the recovery of the velocity. The clutter filtering algorithm starts failing first at the locations where the clutter and the signal overlap, i.e., at v_{in}=±20 and ±40 m s^{-1} as can be seen in Fig. 3.9. At these points the initial velocity estimate has an error greater than v_a/5, and hence the bias removal algorithm fails. The drop off at the extreme ends, ±50 m s^{-1}, is because of the aliasing. This kind of failure mode does not produce progressively increasing standard error. Thus we cannot put an upper limit to the standard error of the estimated velocity to define a cut off point. The standard error suddenly jumps because of the non-resolution of the ambiguity in the velocity estimate. Therefore, it is thought appropriate to exclude outliers in computing the standard error shown in the figure; a limit of velocity recovery is determined by putting a threshold of 10 per cent on the outliers. This is termed as *loss* expressed in percentage. In computing this *loss*, simulations are run with input velocities uniformly distributed over the entire unambiguous interval, $\pm v_a$, and the number of times the recovered velocity falls outside the interval $v_{in}\pm v_a/5$ is counted and expressed as a percentage of the total number of simulations. Generally these outliers fall predominantly in the spectrum overlap regions. (The outliers near the Nyquist velocity are not as detrimental because these can be corrected, nonetheless they are included in the *loss*.) In other regions the velocity is recoverable. The loss parameter is a function of the CSR, number of samples, clutter filter width etc. The CSR=35 dB in Fig. 3.9 is almost at the limit of velocity recovery with a *loss*=7.97% for the von

Hann window. An optimum clutter filter width of n_c=9 coefficients is used.

For the same set of simulation parameters, if {von Hann}^{2} window is used, we have a better velocity recovery performance (Fig. 3.10). The *loss* is reduced to 2.43%. The optimum clutter filter width is 7 coefficients for this window, which corresponds to $\zeta=w_f/w_c$=31.25. It is obvious from Fig. 3.6 that for this filter width {von Hann}^{2} window is better, and the results of simulation confirm this fact. Fig. 3.11 shows the effect of increasing the number of samples to 64. The velocity is recovered fully (*loss* is only 0.15%, mainly due to aliasing) even for a CSR=50 dB, with a much narrower filter width $\zeta=w_f/w_c$=24.6 (n_c=11 coefficients).

The performance of the clutter filtering algorithm is evaluated using a large number of simulations, and the results are tabulated in four tables, 3.3a to 3.3d, where optimum filter widths are used. The simulations are run with increasing clutter filter width, n_c, and the best is selected as the optimum value. For lower values of filter width, the estimated velocity gets biased towards the zero Doppler, as the clutter suppression is not enough to give a reasonable SNR_e after filtering. At larger than the optimum filter widths, the *loss* increases. The optimum is selected manually based on the results, and only these optimum results are shown in the tables. The last column is the *loss* parameter. If we use a limit of 10% for the *loss*, it is easy to determine the upper limit of CSR for a given spectrum width of the signal. Comparing the tables 3.3a and 3.3b for M=32 with von Hann and {von Hann}^{2} windows, respectively, it is clear that the second window performs better. For the CSR values used, the optimum filter widths are fairly wide. Only for n_c=5 or less, the first window is better, i.e., for low CSR values. For M=64 (tables 3.3c and 3.3d), similar conclusions can be drawn, except that the algorithm is able to recover velocities for much higher CSR.

The results in the four tables referred to above are presented in the graphical form to facilitate the selection of optimum filter width for a given situation. Figs. 3.12 to 3.15, show the optimum filter width as a function of CSR, with spectrum width as a parameter (i.e., plot of column 3 versus column 2 of the tables). The next four, Figs. 3.16 to 3.19, are plots of *loss* versus the CSR. The *loss* increases sharply with increasing CSR for the von Hann

window, but for the {von Hann}^{2} window, the increase is much slower. This behavior is seen for both values of M, 32 and 64.

The standard error in the velocity estimate (excluding the outliers) as a function of CSR is given in Figs. 3.20 to 3.23. In the case of the von Hann window, the *sd(v)* increases with increasing CSR because of inadequate filtering of the ground clutter. The side lobes of the ground clutter spectrum give rise to a poorer SNR after filtering. With the {von Hann}^{2} window, the side lobe power is reduced considerably, hence a better SNR is achieved after filtering, which is the reason for *sd(v)* remaining nearly constant with increasing CSR.

3.3.3. Conclusions

An exhaustive simulation of spectral parameter estimation, without and with different window functions, was carried out. In the absence of ground clutter some important observations are the following. The best mean power estimates are obtained with the staggered PRT samples directly. The mean power estimates obtained from the reconstructed spectrum (after the magnitude deconvolution procedure) have biases as well as a larger standard error. The larger is the power loss due to the window, the larger is the error. The velocity estimate is the best without the window, and the increase in the standard error with window depends on the loss of power associated with the window. Only for the spectrum width estimation the window produces improvements, especially in the bias error. The width estimator given by the equation (6.27) of Doviak and Zrnic (1993), which has the lowest standard error, along with the {von Hann}$^{1/4}$ window is the best combination. While the increase in the *sd(w)* is related to the loss of power due to the window, the bias error is a function of the spreading of the spectrum. The {von Hann}$^{1/4}$ window also keeps the degradation of the velocity estimate to a small value, thus, we can use the same window for both velocity and width estimation, which reduces the computation.

In the presence of the clutter, applying the window becomes necessary to contain the spreading of the clutter power, which prevents effective clutter filtering. There is an optimum clutter filter width for a given CSR and signal spectrum width. This optimum filter width is different for different window functions. For large CSR requiring wider clutter

filter, the {von Hann}^{2} window is found to perform better than the von Hann window. For normalized clutter filter widths of less than about 20, the von Hann window performs better.

4. Unambiguous range extension by overlaid signal separation

In the staggered PRT sampling "one-overlay" situation occurs if weather echoes extend to a maximum range, r_{a2}, corresponding to the delay time T_2. Fig. 4.1 shows a part of the PPI radar display for some typical parameters. For example, in the figure the first trip echo from a cell at 50 km and the second trip echo from a cell at 200 km, along a radial arrive at the same time at the radar. In general, the sample at delay time τ and $(T_1+ \tau)$ will overlap after T_2 pulse transmission. After the T_1 pulse transmission there is a clear range of r_{a1} without any overlay. We divide r_{a2} into three regions corresponding to the delay time $\tau \le T_u$, $T_u \le \tau \le 2T_u$, and $2T_u \le \tau \le 3T_u$. Signals from range gates corresponding to region-1 and region-3, require special processing whereas the ones coming from region-2 do not. There can also be ground clutter mainly in the region-1. The ground clutter region is usually insignificant for elevations higher than about 5°.

Note that echoes region-3 for T_1 pulse transmission overlap with echoes from the region-1 for the T_2 pulse transmission. Hence, only half the number of overlaid echo samples are available for these gates. However, if T_u is made an integer multiple of delay time $\delta\tau$, corresponding to the gate spacing (and also τ is made an integer multiple of $\delta\tau$) , for every gate at τ in the region-3 there would be a corresponding gate at $(\tau\text{-}2T_u)$ in the region-1. Therefore, we can get two samples for gates in the region-3 also, but one half of these samples contain overlaid echoes. The other half of the samples do not have overlay. For close-in ranges in the region-1 there can be ground clutter, which also will affect the overlaid signals from region-3.

The separation of these overlaid echoes and clutter filtering appeared to be tractable, and motivated us to examine this situation in more detail. In practice, several different combinations of the clutter, signal, and overlay can occur, and the computations have to be appropriately channeled in the staggered PRT algorithm. The algorithm for the no-overly situation with or without clutter has been treated earlier in section-3 (and in Report 3). In

this section, first we examine the one-overlay problem and develop a method for estimating the spectral moments of both the range gates involved. Later, we also address the situation where the ground clutter is present.

4.1. One-overlay resolution

Figure 4.2 shows the staggered PRT sampling scheme for one-overlay situation. As mentioned in section 4.0, the sample spacing, $\delta\tau$, (gate spacing) is chosen such that T_u, and τ are integral multiples of $\delta\tau$, so that there are $M/2$ common samples for region-1 and region-3. These common samples can contain overlaid echoes whereas the other half of the samples can not. T_u is the basic PRT from which T_1 and T_2 are derived; $T_1 = 2T_u$, $T_2 = 3T_u$, for the stagger ratio, $\kappa = 2/3$, which is used for all results in this section. The transmission sequence starts with T_2 pulse separation (i.e.,T_2 T_1 T_2 T_1 ...); the reason for this choice will be clear later when we discuss the processing algorithm. The sample sequence with a delay time τ (sampled by range gate (a)) is denoted by [v_1, v_2, v_3, v_4, ...etc.], and the samples at delay time ($T_1+\tau$, i.e., rage gate (b)) are represented by [v_1', v_3', v_5', v_7', ...etc.] Note that this set has only odd numbered samples available and these are within the T_2 pulse separation. The first sequence corresponds to the staggered PRT samples of range gate (a) and its odd numbered samples contain overlaid echo corresponding to range gate (b). Similarly, we can form the staggered PRT sequence for the range gate (b) by replacing the even numbered samples in the first set with the second set of samples, i.e., v_1, v_1', v_3, v_3', v_5, v_5', ...etc. The odd numbered and un-primed samples are the common samples and have contribution from ranges corresponding to both gates (a) and (b).

Now, to convert these non-uniform sequences into uniform sequences, we insert zeros in place of missing samples. The code sequence for the gate (a) sequence is [10010...] and for the gate(b) the sequence is [10100...], (Fig. 4.2b). Let us use the notation p_1, v_1, w_1, for the spectral moments signals sampled by gate (a) and p_2, v_2, and w_2, for the spectral moments of signals sampled by gate (b). To explain the one-overlay resolution algorithm, let us assume that p_2 is larger than p_1, and that we estimate the weaker signal velocity, v_1. If it can be recovered, then the stronger signal velocity can also be recovered, hence, we

concentrate on the weaker signal velocity. The same procedure applies with the sequences interchanged, if the gate (a) signal is stronger.

In order to understand the procedure, first let us examine the spectrum of the code sequences, [10000...], [00010...], which are the two components of the staggered PRT code [10010...], and the corresponding rearranged convolution matrices, $\mathbf{C}_{1r}$, $\mathbf{C}_{2r}$ such that $\mathbf{C}_{1r}+\mathbf{C}_{2r}= \mathbf{C}_{r}$. (see Report 3 for the definition and construction of the rearranged matrix). They are given by

$$abs\{\mathbf{C}_r\} = \begin{bmatrix} 1.0 & 0.309 & 0.809 & 0.809 & 0.309 \\ 0.309 & 1.0 & 0.309 & 0.809 & 0.809 \\ 0.809 & 0.309 & 1.0 & 0.309 & 0.809 \\ 0.809 & 0.809 & 0.309 & 1.0 & 0.309 \\ 0.309 & 0.809 & 0.809 & 0.309 & 1.0 \end{bmatrix} \tag{4.1}$$

$$phase\{\mathbf{C}_r\} = \begin{bmatrix} 0° & -72° & 36° & -36° & 72° \\ 72° & 0° & -72° & 36° & -36° \\ -36° & 72° & 0° & -72° & 36° \\ 36° & -36° & 72° & 0° & -72° \\ -72° & 36° & -36° & 72° & 0° \end{bmatrix} \tag{4.2}$$

$$abs\{\mathbf{C}_{1r}\} = abs\{\mathbf{C}_{2r}\} = \begin{bmatrix} 0.5 & 0.5 & 0.5 & 0.5 & 0.5 \\ 0.5 & 0.5 & 0.5 & 0.5 & 0.5 \\ 0.5 & 0.5 & 0.5 & 0.5 & 0.5 \\ 0.5 & 0.5 & 0.5 & 0.5 & 0.5 \\ 0.5 & 0.5 & 0.5 & 0.5 & 0.5 \end{bmatrix} \tag{4.3}$$